Seismic fragility analysis of a long-span cable-stayed bridge equipped with a horizontal bidirectional hybrid damping system

Article Information

Article Type:	Research Article
Section Heading:	
Journal Title:	Structure and Infrastructure Engineering
Publisher:	Taylor & Francis
DOI Number:	10.1080/15732479.2025.2538786
Volume Number:	0
Issue Number:	0
First Page:	1
Last Page:	14
Copyright:	© 2025 Informa UK Limited, trading as Taylor & Francis Group
Copyright Holder:	Informa UK Limited, trading as Taylor & Francis Group
License:	
Received Date:	2025-2-10
Revised Date:	2025-6-10
Accepted Date:	2025-7-9

Seismic fragility analysis of a long-span cable-stayed bridge equipped with a horizontal bidirectional hybrid damping system

Left running head: R. HU ET AL.

Right running head: Structure and Infrastructure Engineering

AQ0 Reply to AQ0：The first and last names of authors are structured correctly .

Renkang Hu[a,b]AQ6, Menggang Yang[a], Dongliang Meng[a], Shangtao Hu[c], Raffaele Cucuzza[b,d], Wenxi Wang[e] and Marco Do

Reply to AQ6：
Renkang Hu: https://orcid.org/0000-0002-2993-8954
Dongliang Meng: https://orcid.org/0000-0002-6140-3968
Marco Domaneschi: https://orcid.org/0000-0002-6077-8338

[a]School of Civil En

[b]Department of Structural, Geotechnical and Building Engineering, Politecnico di Torino, Turin, Italy;

[c]Earthquake Engineering Research and Test Center, Guangzhou University, Guangzhou, China;

[d]College of Civil Engineering, Henan University of Technology, Zhengzhou, Henan Province, China;

[e]Key Laboratory for Bridge and Wind Engineering of Hunan Province, College of Civil Engineering, Hunan University, Changsha, China

Footnotes

No author footnotes is available

Corresponding Author

CONTACT Marco Domaneschi marco.domaneschi@polito.it Department of Structural, Geotechnical and Building Engineering, Politecnico di Torino, Turin, 10129, Italy.

Abstract

This study evaluates the longitudinal and transverse seismic fragility of a long-span bridge equipped with a novel integrated Horizontal Bidirectional Hybrid Damping System (HBHDS). The HBHDS is composed of eddy current dampers, metallic yielding dampers, fuse-lock devices and a spherical steel bearing. A total of 100 ground motions are selected and the damage states of critical components i.e., bearings, towers and piers are defined. Seismic fragility curves for the bridge equipped with the HBHDS are generated at both the component and system levels. Fragility mitigation effects are assessed and compared with those related to the damping system applied to the actual bridge. The results indicate that, at the component level, the proposed HBHDS can achieve a comparable seismic fragility control effect with respect to the as-built bridge configuration in the longitudinal direction. It is also less vulnerable to side pier and tower failure than the transverse fixed system. For the system-level seismic fragility, the HBHDS is the best performer in terms of mitigating the failure probability of a long-span cable-stayed bridge, highlighting superior performance in the longitudinal and transversal direction.

KEYWORDS

Failure probability; fixed system; fluid viscous damper; hybrid damping system; long-span bridge; seismic fragility analysis; vibration control

1. Introduction

Long-span bridges are vital components of transportation networks. However, due to their long fundamental period and inherently low structural damping, long-span bridges are particularly vulnerable to challenges such as component damage or even failure when subjected to severe earthquakes (Domaneschi et al., 2015; Hu et al., 2022; Xiao et al., 2025). For example, during 1988 Saguenay earthquake, one anchorage plate used to connect the girders to an abutment of the cable-stayed bridge failed due to the stress increments induced by the seismic event (Filiatrault et al., 1993a, 1993b). During the 1999 Taiwan earthquake (Chang et al., 2004), significant damage was reported to the tower, superstructure, and some cables of a single-pylon cable-stayed bridge. Due to such occurrences, it is imperative to develop efficient strategies to control and protect long-span bridges from earthquake-induced damages.

Over the past few decades, numerous studies have focused on mitigating the seismic-induced responses and reducing the damage risks of long-span bridges through the use of hybrid passive damping systems. For example, a longitudinal combined damping system, integrating a fluid viscous damper (FVD) and a metallic yielding damper (MYD), has been developed to effectively reduce seismic-induced damage in long-span bridges (Hu et al., 2023c, 2024d). Additionally, a transverse hybrid damping system, combining one transverse steel damper with two sliding spherical steel bearings, has been proposed and validated for seismic protective design in long-span bridges (Zhou et al., 2019). To achieve bidirectional seismic resistance, a multi-directional damping system, consisting of four viscous dampers placed diagonally, was proposed and successfully implemented in an actual long-span bridge (Chen et al., 2023).

Although the aforementioned hybrid damping systems have proven effective in mitigating undesirable seismic responses, their limitations cannot be overlooked. On one hand, these systems primarily focus on mitigating either longitudinal or transverse seismic responses, without simultaneously addressing the combined effects of horizontal directions. On the other hand, the potential for fluid leakage in viscous dampers within the installed damping system poses a significant risk; such failures could compromise the seismic performance of the long-span bridge, leading to inadequate protection during seismic events (Hu, Yang, & Meng, 2023a, 2023b, 2025c). To address these limitations, this study proposes a horizontal bidirectional hybrid damping system (HBHDS) for multi-level vibration mitigation of long-span bridges. This system is designed to address the limitations of existing methods by simultaneously mitigating seismic responses in both horizontal directions (Yang et al., 2024). The proposed HBHDS consists of a spherical steel bearing (SSB), eddy current dampers (ECDs), fuse-lock devices (FLDs), and metallic yielding dampers (MYDs). The system's parameter design and robustness were investigated for application to a long-span cable-stayed bridge subjected to near-fault pulse-like earthquakes (Hu et al., 2024).

Fragility curves are commonly adopted to estimate the probability of structural damage under varying earthquake intensity measures, serving as an essential tool to assess infrastructure vulnerability (Hu et al., 2022; ~~Meng, Liu, & Yang, 2023;~~ Suzuki & Iervolino, 2020; Wei et al., 2024). In view of the bridges equipped with damping system, Xiang and Alam (2019) conducted seismic fragility analysis for bridges equipped with various damping measures. The comparative results revealed that shape memory alloy cables are the most effective in reducing seismic vulnerabilities. Casciati et al. (2008) evaluated the seismic risk of a cable-stayed bridge retrofitted with different passive control damping devices using fragility curves, providing a comprehensive assessment of the performance of such retrofitting strategies. They highlighted the importance of accurately defining the limit states for retrofit techniques. Guo et al. (2023) investigated the influences of the damping system's parameter on fragility functions by the developed seismic fragility analysis framework.

Previous studies have demonstrated that seismic fragility analysis is an effective method for evaluating the seismic performance of long-span bridges, both with and without damping devices, under earthquakes of varying intensities. However, the seismic fragility analysis of the proposed damping system has not yet been conducted, leaving a critical gap in the assessment of its effectiveness and reliability under seismic events. Therefore, the present study aims to evaluate the proposed HBHDS' damage mitigation effectiveness based on the seismic fragility analysis. First, the configuration and working mechanism of the proposed hybrid damping are briefly introduced. Subsequently, based on the Cloud Analysis, a suite of 100 ground motions is selected and the damage states of critical components, i.e., bearings, towers, and piers, are defined. Finally, seismic fragility analysis of the cable-stayed bridge equipped with HBHDS is conducted at both the component and system levels, using fragility functions. Moreover, the mitigation effects of the proposed system are assessed and compared with the performance of damping systems currently applied to the bridge in the longitudinal and transverse directions.

2. Horizontal bidirectional hybrid damping system

The Horizontal Bidirectional Hybrid Damping System is an integrated device, as shown in Figure 1. It can simultaneously control multi-level earthquake-induced vibrations in both the longitudinal and transverse directions, but also address malfunctions, such as fluid leakage, that may occur in FVDs; instead, ECDs are used in the HBHDS to dissipate energy (Zhang et al., 2020).

Figure 1. Configuration of: (a) HBHDS (horizontal bidirectional hybrid damping system), (b) SSB (spherical steel bearing), (c) ECD (eddy current damper), (d) FLD (Fuse-Lock device), and (e) MYD (metallic yielding damper).

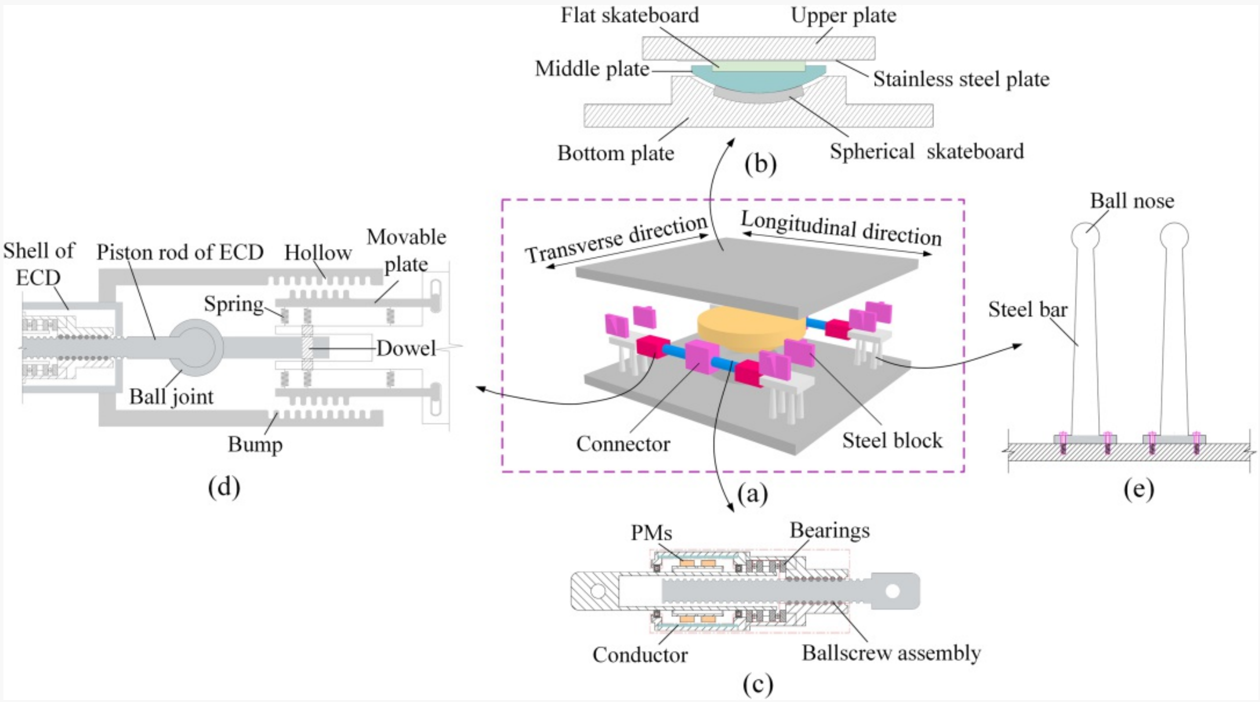

In the longitudinal direction, the ECD and the MYD are expected to dissipate seismic energy due to low- and high-intensity earthquakes, respectively. The FLD is placed in series between the ECD and the MYD, and it can switch the working status of the two dampers according to the force of the ECD and the locking force of FLD. Specifically, when the damping force is smaller than the locking force under low-intensity earthquakes, the ECDs dissipate the input energy by the way of eddy current-damping torque. The FLD remains in its original state, acting as a rigid link and the MYD with enough stiffness remains in an elastic state and acts as a fixed end, as shown in Figure 2(a).

Figure 2. The working mechanism of HBHDS in the: (a) longitudinal direction under low-intensity earthquakes, (b) longitudinal direction under high-intensity earthquakes, and (c) transverse direction.

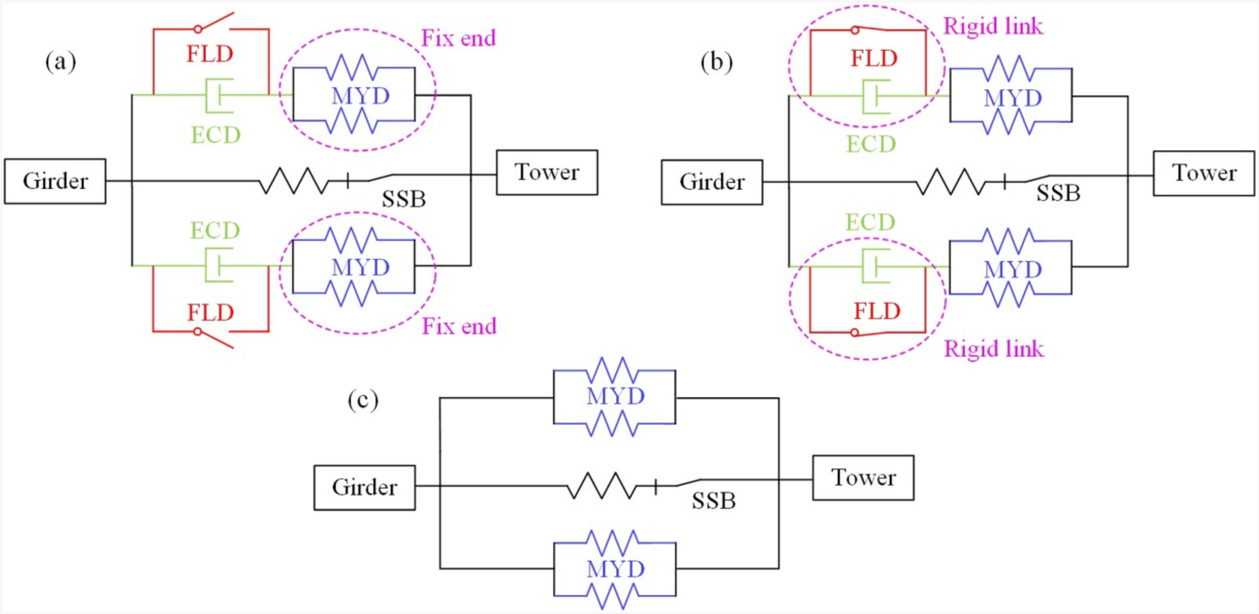

In contrast, the FLD will be triggered under high-intensity earthquakes because of the larger damping force in comparison to the locking force. Then, the MYD starts to dissipate energy by inelastic deformation replacing the ECD. In this case, the out-of-service ECD and the activated FLD are both modeled as rigid links, as shown in Figure 2(b). In the transverse direction, the MYD is always used to protect the bridges from both the low- and high-intensity earthquakes (see Figure 2(c)). It should be noted that, following a major earthquake, the FLD must be re-centered and the yielding MYDs should be promptly replaced in order to ensure adequate protection of the bridge against potential aftershocks. More details of the configuration and working mechanism of the hybrid damping system can be found in Yang et al. (2024), Hu, Hu et al. (2023) and Hu et al. (2024).

The force-displacement curves of the proposed damping system under harmonic loads in the horizontal direction are depicted in Figure 3. The hybrid system exhibits two different working states in the longitudinal direction: only one hysteretic loop is shown in Figure 3(a), which means that the ECD only is working, while two different hysteretic loops are presented in Figure 3(b), indicating that the MYD is active (replacing the ECD) because of the FLD activation. In the transverse direction, a stable hysteretic loop is observed in Figure 3(c), indicating that both the MYD and SSB effectively function.

Figure 3. The Force-displacement relationship of the HBHDS in the: (a) longitudinal direction under low-intensity earthquakes, (b) longitudinal direction under high-intensity earthquakes, and (c) transverse direction.

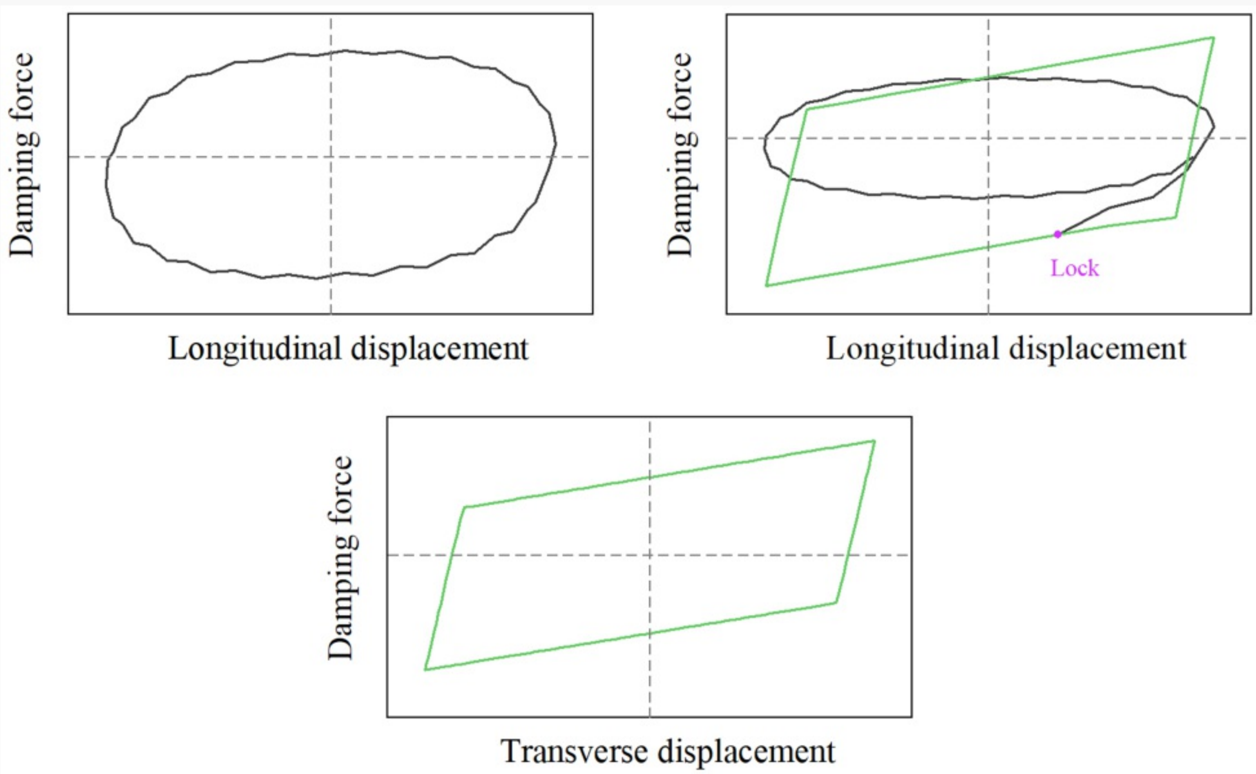

3. Bridge structure and modeling

3.1. The structure

A symmetrical cable-stayed bridge is selected in this study, which is an as-built long-span bridge located in China with a main and side span lengths of 1088 m and 300 m, respectively. As shown in Figure 4(a), 272 cables are symmetrically arranged in two planes following a semi-fan configuration. Among them, the longest one consists of 570 m. The cable spacing is 12 m on the side spans and

16 m on the main span. The girder is a streamlined closed steel box with 41 m width and 4 m height at central span (Figure 4(b)). The damping ratio is approximately 3%. The bridge features two reinforced concrete inverted-Y-shaped towers with a height of 300.4 m. The bottom section of the tower constructed using C50 is shown in Section 1 in Figure 4(c). The piers with hollow section of the bridge are 60.8 m height. They are constructed by C40 concrete and its sections are shown in Section 2 in Figure 4(d). As shown in Figure 4(e), the sliding bearings installed at the piers allow the deck to move in the longitudinal direction. In addition, nonlinear viscous dampers were used between the tower and deck for the longitudinal anti-seismic design. For the sake of wind resistance in the transverse direction, wind-resistance bearings are applied between the tower and deck.

Figure 4. Structural configuration and constraint system of the bridge: (a) elevation view of the bridge, (b) cross section, (c) the tower, (d) the side pier, and (e) the constraint system (units: m).

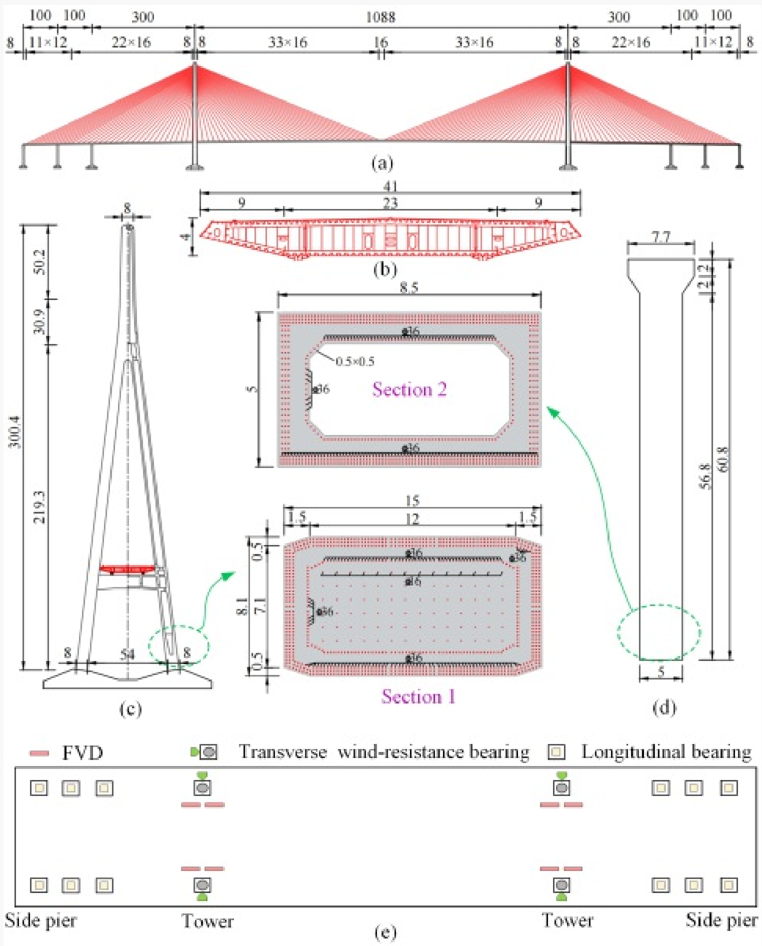

3.2. The finite element model considering plastic hinges

The three-dimensional finite element model (FEM) of the long-span cable-stayed bridge (see Figure 5) was established in the finite element program ANSYS (Ismail et al., 2013). The box girder is modeled using Beam4 elastic beam elements, because it is expected to remain elastic during earthquakes. Cables are modeled with Link10 elements using a modified modulus of elasticity, following the Ernst approach (Ernst, 1965).

Figure 5. Details of the finite element model of the bridge and the HBHDS.

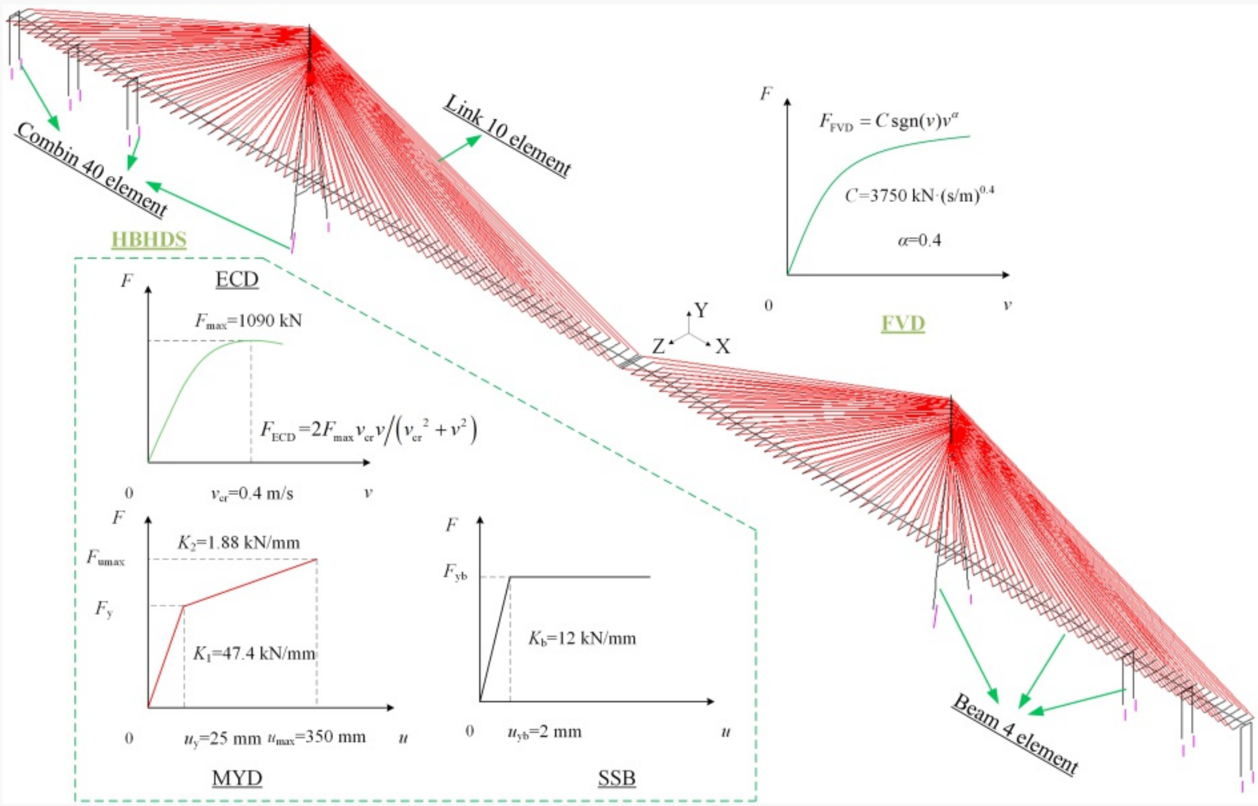

Considering the potential for plastic damage in towers and piers during severe earthquakes, plastic hinges are assumed to form at the base of the bridge towers and piers in the numerical model. The remaining portions of the towers and piers are assumed to remain elastic and are modeled by Beam 4. To obtain the property parameters of the plastic hinges, moment-curvature (*M*-*φ*) analyses are performed according to the bottom sections of the towers and piers shown in Figures 4(c and d). Taking the Section 1 of the tower as an example, the transverse bending moment capacity was computed using Xtract software (Chadwell & Imbsen, 2004), as shown by the solid line in Figure 6. Following the principle of equal area of envelope curve, the corresponding equivalent bilinear model is calculated and plotted using the dashed line. *M*–*φ* analysis results of the towers and piers are summarized in Table 1. In the FEM, the equivalent bilinear model is implemented using Combin40 elements to represent plastic hinges (Meng et al., 2023).

Figure 6. The moment–curvature (M–φ) curves of section 1 at the base of the tower.

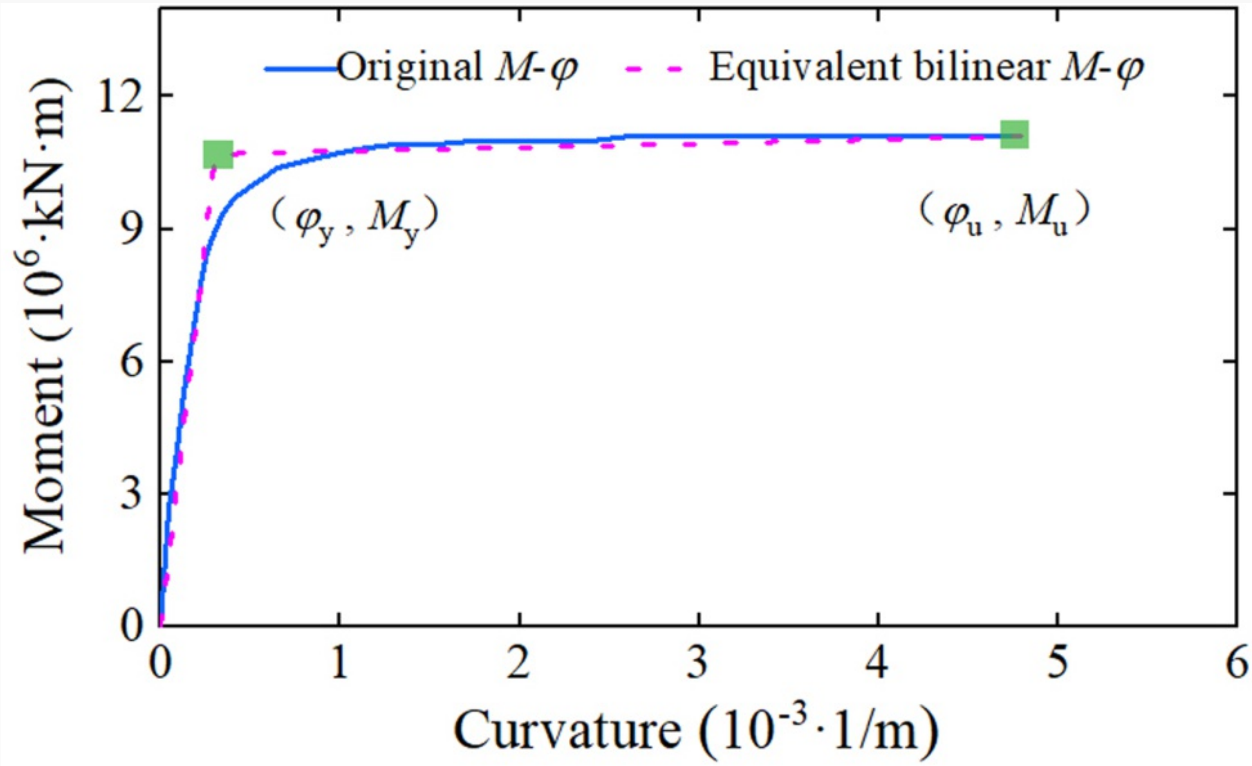

Note: The table layout displayed in 'Edit' view is not how it will appear in the printed/pdf version. This html display is to enable content corrections to the table. To preview the printed/pdf presentation of the table, please view the 'PDF' tab.

Table 1. *M–φ* analyses of the tower and the pier.

Parameters	Section 1 of the tower		Section 2 of the pier	
	Longitudinal	Transverse	Longitudinal	Transverse
φ_y (10^{-3}·m^{-1})	0.5227	0.3011	0.8146	0.573
M_y (10^6·kN·m)	5.992	10.701	1.658	2.547
φ_u (10^{-3}·m^{-1})	10.692	4.798	21.806	7.151
M_u (10^6·kN·m)	6.134	11.095	1.699	2.693

Place the cursor position on table column and click 'Add New' to add table footnote.

The soil–structure interaction (SSI) effects for piles and towers were not included, and fixed-base conditions were assumed (Guo et al., 2022). Based on the modal analysis of the cable-stayed bridge, the first three frequencies were identified as 0.048, 0.064, and 0.112 Hz, in transverse, longitudinal, and vertical directions, respectively. The modal results are consistent with those presented in a previous study (Wang et al., 2013).

3.3. Simulation of damping systems

To analyze the seismic performance of the bridge in the longitudinal direction using the proposed novel system, three cases have been compared: (i) Case 1: the conventional bridge arrangement as floating system (uncontrolled configuration). (ii) Case 2: the bridge equipped with the proposed HBHDS. (iii) Case 3: the bridge incorporating the actual configuration with FVDs. In detail, four nonlinear FVDs were applied in longitudinal direction at each tower-deck connection of the as-built bridge in Case 3 (Figure 4(e)), while two sets of HBHDS were installed replacing four FVDs in Case 2. In the transverse direction, the performance of the bridge with HBHDS (Case 2) is compared to the bridge with traditional wind-resistance bearings (Case 3) and the uncontrolled arrangement (Case 1). In Case 3, the adopted transverse constraint system of the actual bridge configuration, with FVDs in the longitudinal direction, is simplified as a fixed system (FS) for the numerical finite element simulations. Table 2 summarizes all the bridge configurations in both the longitudinal and transverse directions.

Note: The table layout displayed in 'Edit' view is not how it will appear in the printed/pdf version. This html display is to enable content corrections to the table. To preview the printed/pdf presentation of the table, please view the 'PDF' tab.

Table 2. Cases of considering damping system in the longitudinal and transverse directions.

Direction	Case	Damping system
Longitudinal	1	Uncontrolled (floating)
	2	With HBHDS
	3	With FVD
Transverse	1	Uncontrolled (floating)
	2	With HBHDS
	3	With FS

Place the cursor position on table column and click 'Add New' to add table footnote.

For the proposed HBHDS, both the MYD and the SSB were modeled using the bilinear model described in Park and Otsuka (1999), as shown in Figure 5. The yielding force, yielding stiffness and postyielding stiffness are the critical parameters to represent their mechanical behavior. The nonlinear force-velocity behavior of the ECD was simulated following the Wouterse model (Wouterse, 1991) expressed in Figure 5. It was directly applied to the associated connected elements whose velocity is computed and inserted into the Wouterse model at each iteration. Regarding the simulation of FLD, it can be reproduced by automatically comparing the designed locking force and the ECD damping force computed at each iteration. In other words, when the damping force does not exceed the locking force, the damping force is applied to the tower and girder, while the elements of the MYD are directly engaged. All parameters of the HBHDS in Figure 5 were optimized as reported by Yang et al. (2024). For the FVD, the Combin 37 element in ANSYS was used to simulate the damper's mechanical behavior. Its parameters can be found from the public literature (Guo et al., 2015). Additionally, the FS is implemented by assigning fixed constraints, whereas constraints in the corresponding direction are released for the uncontrolled system.

4. Methodology for seismic fragility analysis

4.1. Input ground motions and intensity measures

Incremental Dynamic Analysis (IDA) and Cloud Analysis are commonly used to derive seismic fragility curves (Li et al., 2021; Zentner et al., 2017). These curves can express the failure probability of components or structures under different earthquake intensity measures (IMs). IDA is performed by matching spectra and then scaling the records in amplitude successively to high intensity levels until failure is achieved. However, scaled records may not capture the key features of unscaled ground motions at the same intensity (Jalayer et al., 2017). The Cloud Analysis is well known for the simplicity of its linear regression formulation in logarithmic scale between the maximum structural responses and the corresponding IMs. Unlike IDA, it requires fewer analyses and does not involve scaling ground motions. Therefore, Cloud Analysis using unscaled records is adopted to assess the fragility of long-span bridges with various damping systems.

As mentioned above, a suite of 100 representative ground motions is selected. 80 ground motions extracted from the PEER database and 20 ground motions selected from the SAC project database are included. Epicenter distances range from 13 to 60 km, including both near- and far-field earthquakes, with magnitudes from 5.8 to 6.9. The 20 SAC ground motions are horizontal ground motions for Los Angeles with a probability of exceedance of 2% and 10% in 50 years, respectively. (Shafieezadeh et al., 2012). Each ground motion record includes two horizontal components (H1 and H2). Figure 7 shows the individual acceleration and displacement spectrums of selected ground motions and the corresponding mean spectrum. The spectra of the H1 and H2 components are similar. The strongest horizontal component of each ground motion is applied at the bridge supports along the longitudinal axis using the large mass method. This is due to the mechanical behavior of the HBHDS, which can be examined and observed, especially the function of the FLD under lager ground motions. Moreover, the orthogonal imbalance between the H1 and H2 components is not considered in this study. Similarly, the vertical component of ground motion is also excluded from the current analysis.

Figure 7. Acceleration and displacement spectra of the selected ground motions.

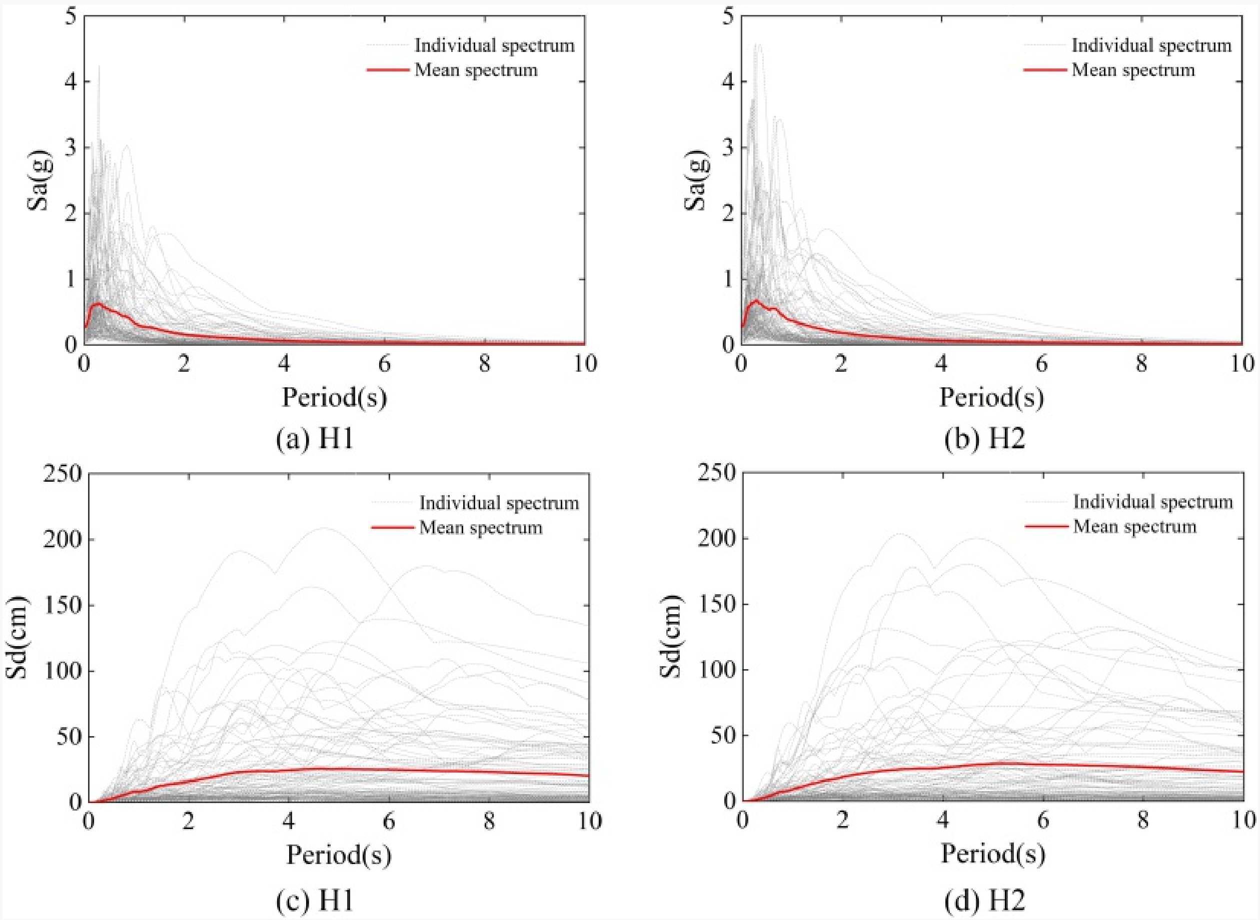

According to the previous studies, the seismic intensity IMs has a significant effect on the accuracy of the seismic response and estimation of the damage exceeding probability (Feng et al., 2018). Peak ground acceleration, peak ground velocity (PGV) and first-mode spectral acceleration are the most commonly used IMs (Ma et al., 2019; Wu et al., 2016). Recent studies (Wei et al., 2020; Zhong et al., 2019) suggest that PGV is the most suitable IM for long-span cable-stayed bridges due to its practicality and reliability. Therefore, PGV is selected in this study as the intensity measure for the fragility analysis.

4.2. Definition of the damage states and engineering demand parameters

According to the previous research (Hazus, 2011), four damage states (DS) of structural components were respectively defined: Slight (DS 1), Moderate (DS 2), Extensive (DS 3) and Complete Damage (DS 4). The present study evaluates the fragility of four structural components: tower bearings, side pier bearings, towers, and side piers. Displacement is used as the damage index for bearings, while rotation ductility is used for towers and piers. The spherical steel bearing (SSB) of the HBHDS is installed in parallel with the MYD, ensuring synchronized movement of all HBHDS components, as described in Section 2. The MYD is considered inoperative when the relative displacement δ_{d1} exceeds its ultimate value of 0.35 m. Consequently, for displacement levels beyond this threshold, the damage states refer solely to the SSB. Following the work of Wei et al. (2020), the SSB damage states are defined by displacement thresholds: 0.35 m (slight), 0.6 m (moderate), 1.0 m (extensive), and 1.5 m (complete).

For the longitudinal sliding bearing at each side pier, the longitudinal displacement (δ_{d2}) is used to define the damage states by referring to the work of Zhong et al. (2023). According to Figure 8, the bearing reaches DS 1 when its displacement exceeds 0.15 m. DS 3 corresponds to the full distance from the bearing centerline to the masonry plate edge; DS 2 is set at half that value. Once the bearing surpasses the ending of the bent cap, namely 0.8 m, complete damage (DS 4) occurs. Note that longitudinal bearings are assumed not to sustain damage in the transverse direction, as there is no relative motion between the tower and girder. For the tower and side pier, the rotation ductility (μ_θ) is defined to describe their damage states. It can be calculated by θ/θ_{y1}, where θ is the maximum rotation response, and θ_{y1} is the rotation corresponding to the first yield curvature φ_{y1}. φ_y can be obtained by moment-curvature analysis of the corresponding sections, as described in Sectio n 3.2. Referring to the research (Wu et al., 2016; Zhong et al., 2023), the rotation ductile values corresponding DS are shown in Table 3.

Figure 8. Damage state of the longitudinal sliding bearing at the side piers.

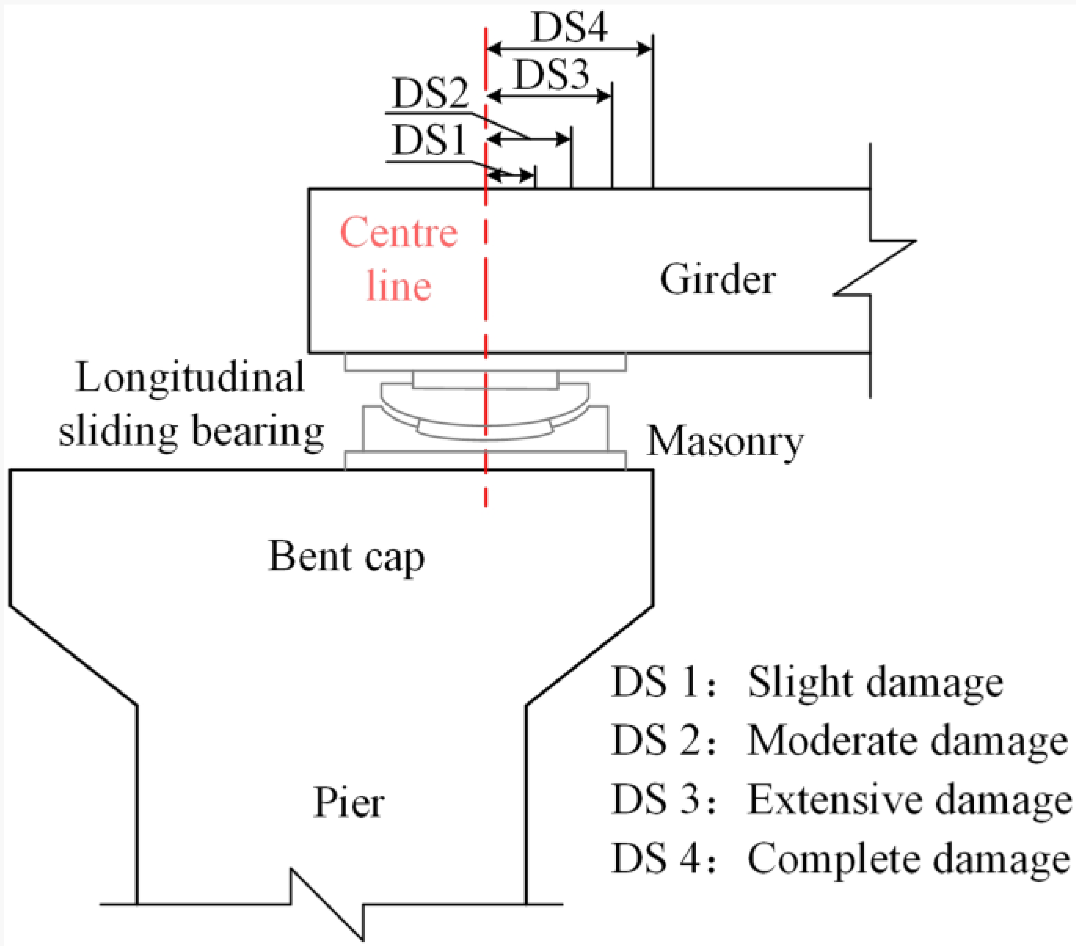

Note: The table layout displayed in 'Edit' view is not how it will appear in the printed/pdf version. This html display is to enable content corrections to the table. To preview the printed/pdf presentation of the table, please view the 'PDF' tab.

Table 3. Median values of different damage indexes.

Component	Damage state				Reference
	Slight DS 1	Moderate DS 2	Extensive DS 3	Complete DS 4	

The displacement of bearings at the tower (m)	δ_{d1} L	0.35	0.6	1	1.5	Wei et al. (2020)
	δ_{d1} T	0.35	0.6	1	1.5	Wei et al. (2020)
The displacement of bearings at the pier (m)	δ_{d2} L	0.15	0.3	0.5	0.8	Zhong et al. (2023)
	δ_{d2} T	/	/	/	/	Zhong et al. (2023)
The rotation ductile of towers	$\mu_{\theta1}$ L	1	2	4	7	Wu et al. (2016)
	$\mu_{\theta1}$ T	1	2	4	7	Wu et al. (2016)
The rotation ductile of piers	$\mu_{\theta2}$ L	1	2	4	7	Wu et al. (2016)
	$\mu_{\theta2}$ T	1	2	4	7	Wu et al. (2016)

In the present study, the displacements of bearings at each tower (δ_{d1}) and pier (δ_{d2}), the rotation ductile of the tower ($\mu_{\theta1}$) and side pier ($\mu_{\theta2}$) are selected as EDPs. Seismic responses are computed for each component using nonlinear time-history analyses in ANSYS. It is assumed that the selected EDP follows the lognormal probability distributions, which is defined as:

$$\ln\,(EDP) = b + a\,\ln\,(IM)$$

where a and b are the linear regression coefficients. As anticipated at Section 4.1, PGV is selected as the IM to compute the regression coefficients. Table 4 summarizes the regression and R^2

coefficients for each EDP in all cases. Note that the corresponding parameters for the bearing's displacement in the bridge with FS (Case 3) are empty in Table 4. This is because there is no relative motion between the tower and girder due to the transverse fixed constrain. Moreover, the higher R^2 values also reveal that the selected regression model could fit well with the different structural demands.

Note: The table layout displayed in 'Edit' view is not how it will appear in the printed/pdf version. This html display is to enable content corrections to the table. To preview the printed/pdf presentation of the table, please view the 'PDF' tab.

Table 4. Regression coefficients of each EDP for different components of each case.

Direction	EDP	Case	*A*	*b*	R^2
Longitudinal	δ_{d1L}	1	1.13	−5.99	0.68
		2	1.30	−6.84	0.73
		3	1.36	−6.91	0.79
	δ_{d2L}	1	1.15	−5.43	0.77
		2	1.27	−5.89	0.81
		3	1.28	−5.92	0.82
	$\mu_{\theta 1L}$	1	0.84	−10.93	0.71
		2	0.93	−11.12	0.72
		3	0.88	−11.01	0.73
	$\mu_{\theta 2L}$	1	1.15	−12.95	0.90
		2	1.17	−13.01	0.89
		3	1.16	−13.02	0.88
Transverse	δ_{d1T}	1	0.93	−4.85	0.77
		2	1.29	−7.36	0.84
		3	/	/	/
	$\mu_{\theta 1T}$	1	1.16	−12.71	0.79
		2	1.27	−13.08	0.86
		3	1.30	−13.09	0.87
	$\mu_{\theta 2T}$	1	1.16	−13.0	0.89
		2	1.06	−12.78	0.82
		3	0.91	−12.34	0.83

Place the cursor position on table column and click 'Add New' to add table footnote.

4.3. Fragility function

The component-level fragility function represents the conditional probability that the seismic demand (*D*) of the structure reaches or exceeds its capacity (*C*) under a given level of ground motion intensity measure (*IM*). In other words, it is the probability that the engineering demand parameter (*EDP*) reaches or exceeds the defined damage state for a specific *IM*. It can be computed as:

$$P_{\mathrm{f}} = P\left[D \geq C|IM\right] = \Phi\left[\frac{\ln\left(S_D\right) - \ln\left(S_C\right)}{\sqrt{\beta_{D|IM}^2 + \beta_C^2}}\right]$$

where Φ (·) is the standard normal cumulative distribution function; S_D and S_C are the value of median of the component's response and capacity, respectively; β_c is the logarithmic standard deviation of the structural capacity reflecting structural functionality levels associated with defined damage, set to be 0.35 for the components of long-span cable-stayed bridge (Li et al., 2018); $\beta_{D|IM}$ is the standard deviation of the seismic demand that can be computed as:

$$\beta_{D|IM} = \sqrt{\frac{\sum_{i=1}^{N}\left[\ln\left(EDP_i\right) - \ln\left(aIM_i^b\right)\right]^2}{N-2}}$$

where N is the total number of performed nonlinear time history analyses.

The system fragility can be derived from the fragility functions of bridge components using the upper bound formulation of first-order reliability theory (Choi et al., 2004):

$$\max_{i=1}^{n} (P_{fi}) \leq P_S \leq 1 - \prod_{i=1}^{n} (1 - P_{fi})$$

in which P_{fi} and P_s present the failure probabilities of the ith component and of the overall system, respectively; n is the number of the adopted vulnerable components. Eqs. (2) through (4) summarize the analytical procedure used to compute the system-level fragility from component-level performance.

5. Results of the seismic fragility analysis for the long-span bridge

After determining the regression models of EDPs and the probabilistic capacity model, the seismic fragility analysis can be performed for both the component and system levels of the cable-stayed bridge. The longitudinal and transverse seismic fragility curves of the considered components with different damping systems and damage states are developed, respectively. Furthermore, the system-level fragility curves are obtained by integrating the component-level fragilities through the series system model described in Eq. (4).

5.1. Fragility at the component level

5.1.1. Assessment under longitudinal excitations

Figure 9 displays the fragility curves of the tower bearing under longitudinal earthquakes, from slight to complete damage states, for different damping configurations. In general, the implementation of the HBHDS and FVD significantly reduces the fragility of the bearing at the tower at all damage states compared to the uncontrolled bridge. The HBHDS results in lower bearing failure probabilities than the FVD at each damage state. For example, considering the bridge with a floating system (i.e., the uncontrolled case) at a PGV of 150 cm/s, the failure probabilities of the bearing from slight to complete damage states are 0.804, 0.582, 0.342, and 0.184, respectively.

Figure 9. Seismic fragility curves of the bearing at the tower: (a) uncontrolled, (b) HBHDS, and (c) FVD configurations.

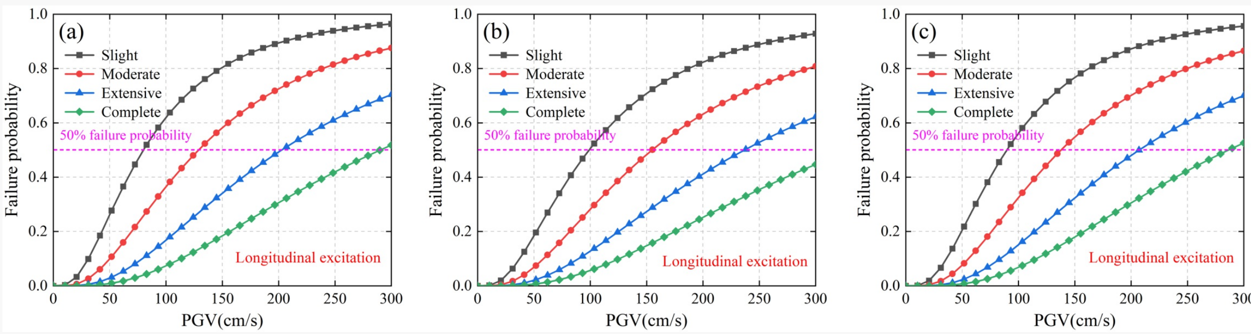

After installing the proposed HBHDS, these probabilities are reduced to 0.707, 0.481, 0.272, and 0.146 for the slight, moderate, extensive, and complete damage states, respectively. The corresponding failure probabilities are reduced by 12.1%, 17.4%, 20.5%, and 20.7%, respectively. When the as-built bridge adopts FVD in practical engineering, the failure probabilities of the bearing at the tower are reduced by 4.9%, 6.2%, 5.3%, and 2.7%. It can also be concluded that the effectiveness of the HBHDS and FVD in reducing the failure probability of the bearing component increases with higher damage states. In other words, both damping systems exhibit significant mitigation effectiveness, particularly for the extensive and complete damage states.

The fragility curves for the longitudinal sliding bearing at the side pier are shown in Figure 10. When experiencing longitudinal ground motions, the failure probabilities of the bearing at the pier are slightly reduced in the cases of installing the HBHDS and FVD. Moreover, the bearing at the pier exhibits higher failure risk compared with the failure probability of the bearing at the tower (see Figur e 9) when the damage state is fixed.

Figure 10. Seismic fragility curves of the bearing at the side pier: (a) uncontrolled, (b) HBHDS, and (c) FVD configurations.

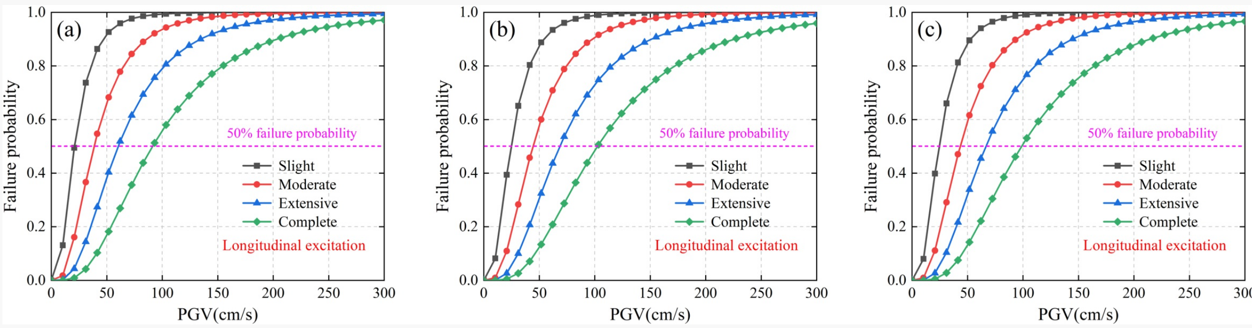

The seismic fragility curves for the tower (sections 1) and the pier (section 2), corresponding to the bridge with different damping systems, are also compared and discussed. As shown in Figures 11 and 12, the failure probabilities of both the tower and side pier for the example bridge with HBHDS and FVD are significantly reduced across all four damage states, especially under slight and moderate damage states. The complete damage of the tower and the side pier cannot appear when the HBHDS and FVD are installed. In addition, the tower is more vulnerable than the section of the side pier under identical damage states in the cases of the bridge adopted same damping system.

Figure 11. Seismic fragility curves of the tower: (a) uncontrolled, (b) HBHDS, and (c) FVD configurations.

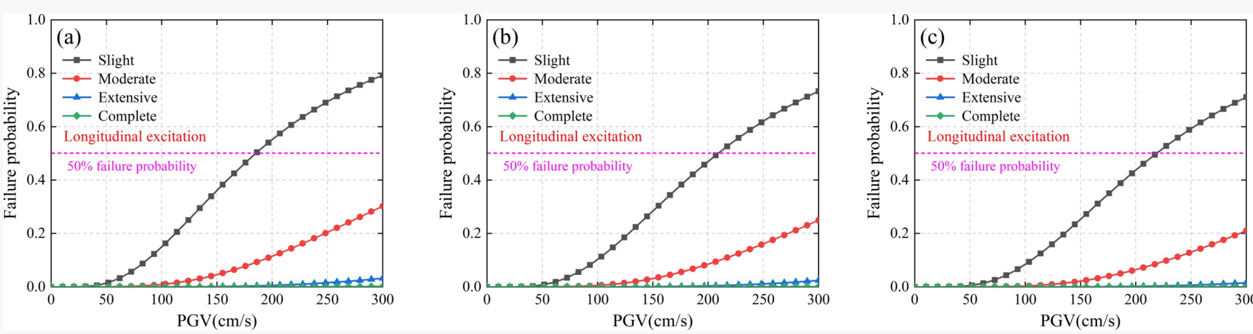

Figure 12. Seismic fragility curves of the pier: (a) uncontrolled, (b) HBHDS, and (c) FVD configurations.

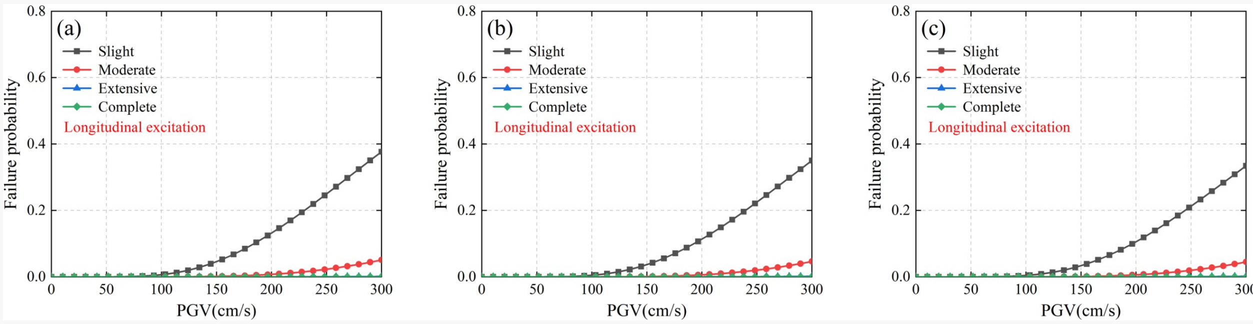

5.1.2. Assessment under transverse excitation

To evaluate the failure probability under transverse ground motion, fragility curves are compared for three configurations: HBHDS (Case 2), fixed system (FS, Case 3), and the uncontrolled case (Case 1). It is important to note that the FS is a simplified representation of the wind-resistance bearing designed to limit transverse displacements in the actual bridge configuration. In contrast, the uncontrolled case, serving as a reference, represents the release of transverse constraints present in the FS. Note that, the damage of the bearing at side piers is not considered because it can only allow to move along the longitudinal direction.

The comparative fragility curves for the bearing at the tower in each bridge configuration under different damage states are shown in Figure 13. Compared to the uncontrolled case, the HBHDS reduces bearing failure probabilities, especially at higher damage states. Specifically, at a PGV of 150 cm/s, the fragilities of the bearing in the HBHDS system are 0.569, 0.341, 0.169, and 0.081 for the slight, moderate, extensive, and complete damage states, respectively. In contrast, for the uncontrolled case, the corresponding fragilities are 0.897, 0.679, 0.388, and 0.188. HBHDS reduces the failure probability by 36.6% to 57.4% compared to the uncontrolled case, depending on the damage state. In Case 3, no bearing damage occurs due to the fixed transverse constraint preventing relative motion.

Figure 13. Seismic fragility curves of the bearing at the tower: (a) uncontrolled, (b) HBHDS bridge configurations.

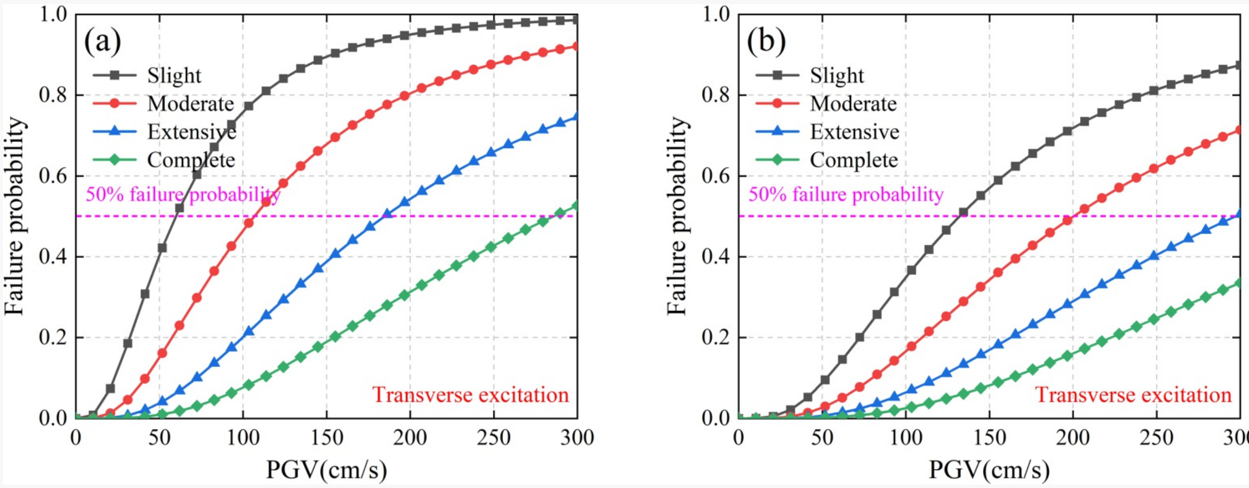

Figures 14 illustrates the seismic fragility curves in terms of the tower at Section 1 for different bridge configurations under transverse excitations. It can be observed that the failure probabilities of tower in the case of the bridge with FS is higher than that of the uncontrolled and HBHDS. This is the drawback for the rigid connection, which transfers all the forces from the deck to the tower. Moreover, the bridge equipped with the HBHDS demonstrates slightly less effectiveness compared to the uncontrolled case, as it introduces a marginally higher failure probability. This is due to the MYD in HBHDS, which increases transverse stiffness when activated during seismic events. For example, the probabilities of the tower damage for the actual bridge with FS at the PGV of 150 cm/s are 0.661, 0.321, 0.093, and 0.0247. By implementing the proposed HBHDS, these values are slightly reduced to 0.589, 0.258, 0.064, and 0.014.

Figure 14. Seismic fragility curves of the tower: (a) uncontrolled, (b) HBHDS, and (c) FS bridge configurations.

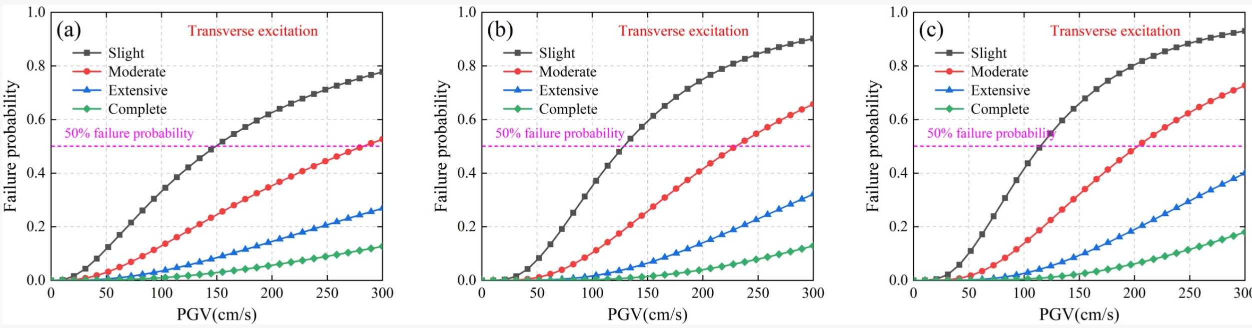

Figure 15. Seismic fragility curves of the pier: (a) uncontrolled, (b) HBHDS, and (c) FS bridge configurations.

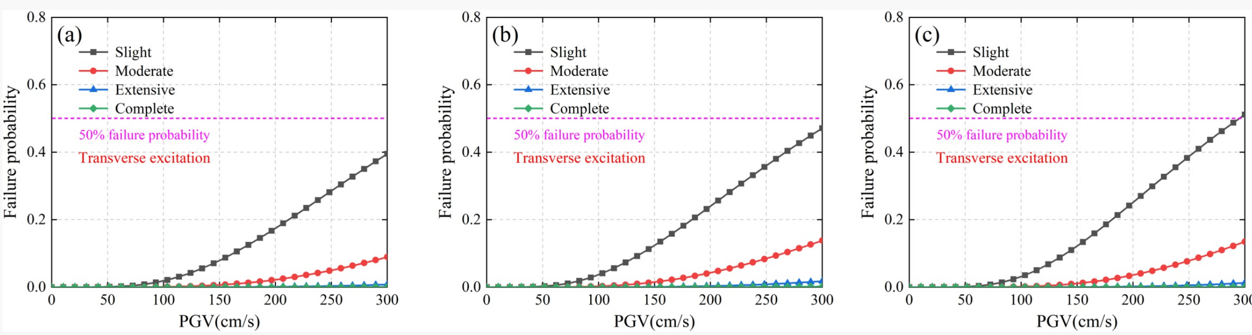

Figure 15 plots the comparative fragility curves in terms of the side pier at Section 2 for different bridge configurations. It can be found that the sequence of efficient system in terms of reducing the failure probabilities of the side pier under slight and moderate damage states is similar to that of the tower shown in Figure 14. In other words, FS is the most vulnerable damping system for the failure of the side pier, the following is HBHDS and uncontrolled case. However, the side piers of the bridge equipped with all damping systems cannot occur complete damage compared to the bridge towers when subjected to transverse earthquakes.

5.2. Fragility at the system level

5.2.1. Assessment under longitudinal excitations

Based on the components' fragilities, system-level fragility curves of the cable-stayed bridge can be determined by Eq. (4), as shown in Figure 16. Both HBHDS and FVD significantly reduce system fragility under longitudinal ground motions, compared to the uncontrolled case. In other word, the uncontrolled system is the most vulnerable system. HBHDS and FVD perform similarly at slight and moderate damage levels, but HBHDS is more effective at extensive and complete states. In general, the proposed HBHDS can achieve the similar or even superior effectiveness in reducing the system-level failure probability of the bridge in comparison to the FVD applied to the actual bridge in the longitudinal direction.

Figure 16. System-level fragility curves of the bridge with different configurations for the: (a) slight damage, (b) moderate damage, (c) extensive damage, and (d) complete damage levels (longitudinal excitation).

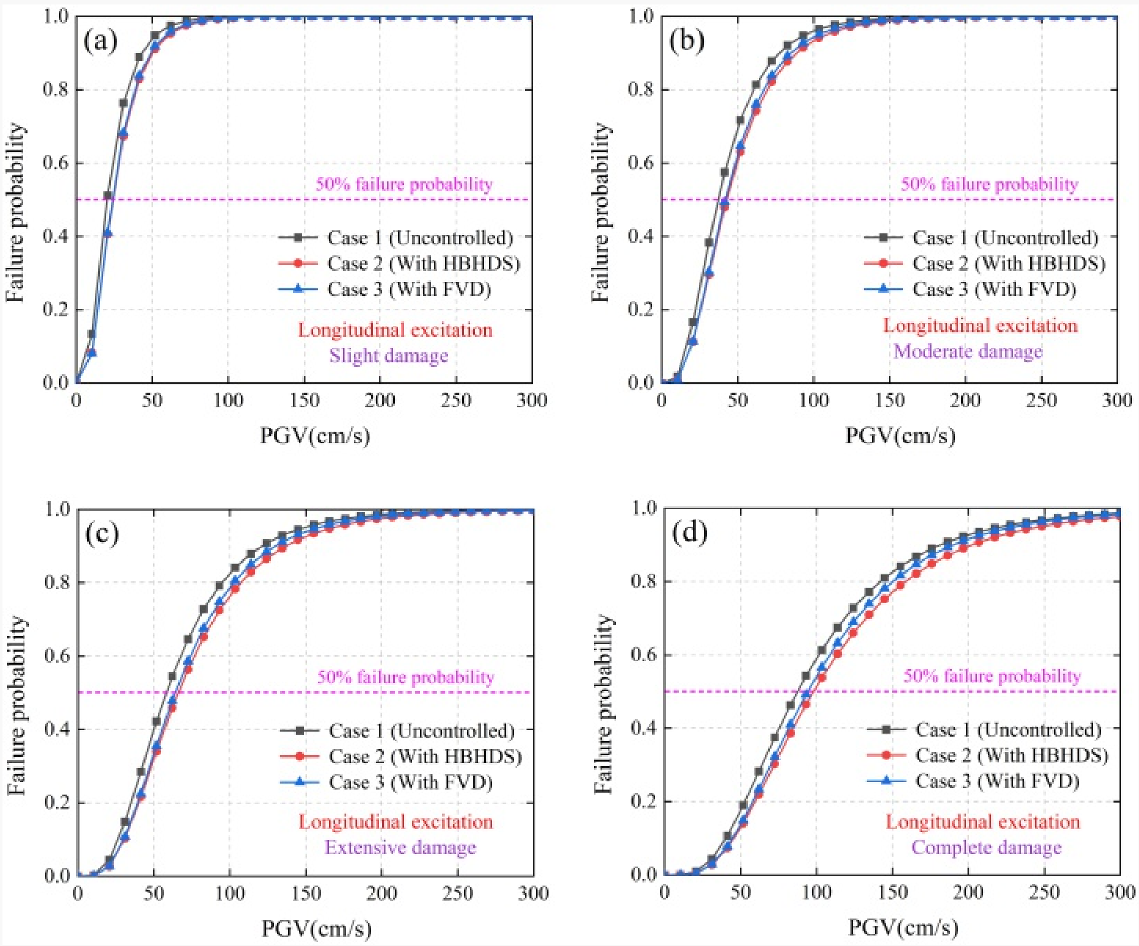

5.2.2. Assessment under transverse excitations

Similarly, the transverse system fragility curves of the bridge in the considered three cases at different damage states are presented in Figure 17. In terms of effectiveness, the damping systems rank as follows: FS (most effective), HBHDS, and uncontrolled (least effective). In other words, Case 3 is the optimal damping system for the complete damage state. This is because the damage of the bearing at the tower in the transverse direction is not considered in Case 3, resulting in a zero-failure probability for that component. With HBHDS, the system failure probabilities at PGV = 100 cm/s are reduced by 11.0% to 66.1% compared to the uncontrolled case. These results confirm the HBHDS is effective in reducing system fragility under transverse ground motion.

Figure 17. System-level fragility curves of the bridge with different configurations for the: (a) slight damage, (b) moderate damage, (c) extensive damage, and (d) complete damage levels (transverse seismic excitation).

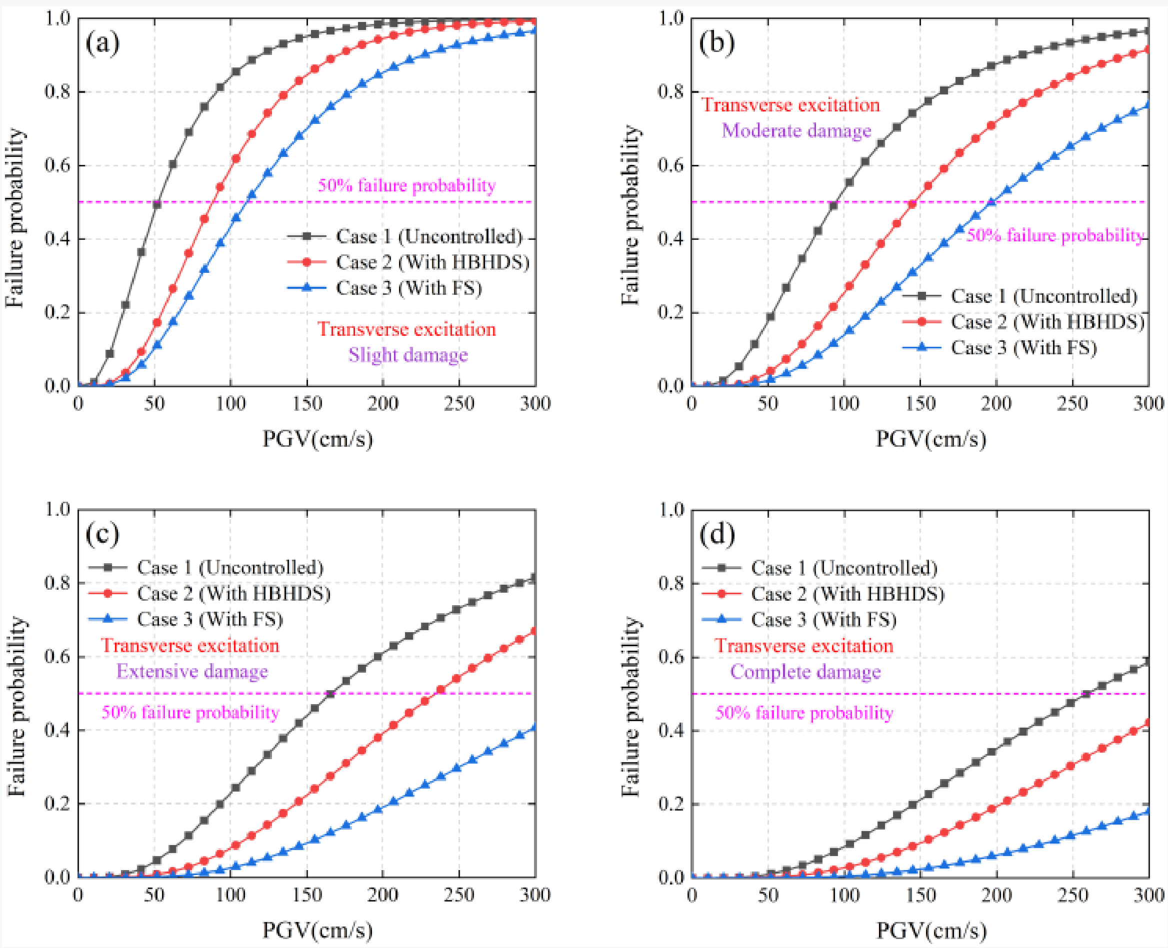

6. Conclusions

The current study investigates the seismic fragility mitigation effectiveness of a long-span cable-stayed bridge incorporating the proposed Horizontal Bidirectional Hybrid Damping System (HBHDS). Fragility curves of critical components and of the overall system are computed. The fragility of the as-built damping systems and the uncontrolled case are also compared with the proposed HBHDS. The following conclusions can be drawn:

1. In the longitudinal direction, the implementation of the HBHDS and FVD can significantly reduce the failure probabilities of the critical components (the bearing at the tower and side pier, the tower and side pier) at all damage states compared to the uncontrolled bridge. Furthermore, the proposed damping system can achieve a comparable seismic fragility control effect with respect to the as-built bridge configuration.
2. In the transverse direction, the failure probability of the bearing at the tower for the bridge with the proposed HBHDS can be effectively reduced in comparison to the uncontrolled system. Moreover, the HBHDS is a less vulnerable damping system for the failure of the side pier and tower than the FS applied to the as-built bridge.
3. In terms of the system-level seismic fragility, the proposed HBHDS can achieve similar or even superior effectiveness in reducing the system-level failure probability of the bridge in comparison to the FVD applied to the actual bridge in the longitudinal direction. In the transverse direction, it is also an effective solution to mitigate the fragility of the system.

In summary, the proposed HBHDS demonstrates strong effectiveness in mitigating the seismic fragility of long-span cable-stayed bridges by providing superior control in both the longitudinal and transverse directions. Unlike conventional damping systems that treat directional responses separately, the HBHDS enables simultaneous bidirectional vibration control through its integrated configuration of ECD and MYD components. Therefore, the HBHDS represents a promising solution for enhancing the seismic resilience of long-span bridges under horizontal ground motions.

While this study offers valuable insights, it is currently limited by the use of uniform seismic excitations with a fixed incident angle. Future research will aim to overcome these limitations by investigating the effects of spatial variability, such as wave passage effects, loss of coherency, and site conditions, as well as varying incident angles of bidirectional ground motions, in order to provide a more comprehensive evaluation of the bridge’s seismic vulnerability. In addition, the mechanical behavior of the proposed HBHDS will also be investigated and verified by experiments.

Acknowledgments

The last author gratefully acknowledges the support given by PRIN 2022" BIO-RESTORE–BIO-based Resilient Energy and Seismic RetrofiT of the REsidential building stock", Prot. 202234HM8J, CUP E53C24002680006, Bando Prin 2022 – Decreto Direttoriale n. 104 del 02-02-2022.

Disclosure statement AQ1

Reply to AQ1：All authors agree with the discourse statement

No potential conflict of interest was reported by the author(s).

Funding

This work is supported by the National Natural Science Foundation of China (Grant No. 52278232, 52308224), the China Scholarship Council (Grant No. 202306370151), the Postgraduate Scientific Research Innovation Project of Hunan Province (Grant No. CX20230108), the China National Postdoctoral Program for Innovative Talents (Grant No. BX20230429), the China Postdoctoral Science Foundation project (Grant No. 2023M733970, 2024M750618), and the Postdoctoral Fellowship Program of CPSF (No. GZC20240325). AQ7

Reply to AQ7：The funding information has been resupplied as following:
Renkang Hu: the China Scholarship Council (Grant No. 202306370151)
Menggang Yang: National Natural Science Foundation of China (Grant No. 52278232)
Dongliang Meng: National Natural Science Foundation of China (Grant No. 52308224),
China National Postdoctoral Program for Innovative Talents (Grant No. BX20230429),
China Postdoctoral Science Foundation project (Grant No.
Shangtao Hu: China Postdoctoral Science Foundation project (Grant No. 2024M750618),
the Postdoctoral Fellowship Program of CPSF (No. GZC20240325).

Note: this Edit/html view does not display references as per
to correct this. The content is correct and it will be converted
version.

References

Hu, R., Hu, S., Yang, M., & Zhang, Y. (2022). Metallic yieldin
for vibration control in civil engineering: A review. *Internationa*
Dynamics, 22(16), 2230006. https://doi.org/10.1142/S021945

Reply to AQ2 and AQ3：We decide to delete these citations from the list.

Domaneschi, M., Martinelli, L., & Po, E. (2015). Control of wi
bridge by TMD: Hybridization and robustness issues. *Compu*
https://doi.org/10.1016/j.compstruc.2015.02.031

Xiao, B., Wei, B., Zhao, H., Zheng, X., Zhang, R., Chen, J., & Jiang, L. (2025). Effect of seismic isolation parameters on component damage and running safety performance of high-speed railway bridge-track system under near-fault earthquakes. *Engineering Structures*, *328*, 119712. https://doi.org/10.1016/j.engstruct.2025.119712

Filiatrault, A., Tinawi, R., & Massicotte, B. (1993a). Damage to the cable-stayed bridge during the 1988 Saguenay earthquake. I: Pseudostatic analysis. *Journal of Structural Engineering*, *119*(5), 1432–1449. https://doi.org/10.1061/(ASCE)0733-9445(1993)119:5(1432)

Filiatrault, A., Tinawi, R., & Massicotte, B. (1993b). Damage to cable-stayed bridge during 1988 Saguenay earthquake. II: Dynamic analysis. *Journal of Structural Engineering*, *119*(5), 1450–1463. https://doi.org/10.1061/(ASCE)0733-9445(1993)119:5(1450)

Chang, K., Mo, Y., Chen, C., Lai, L., & Chou, C. (2004). Lessons learned from the damaged Chi-Lu cable-stayed bridge. *Journal of Bridge Engineering*, *9*(4), 343–352. https://doi.org/10.1061/(ASCE)1084-0702(2004)9:4(343)

Hu, S., Meng, D., Hu, R., & Yang, M. (2023). A Combined Viscous-Steel Damping System (CVSDS) for longitudinal vibration mitigation of a long-span railway suspension bridge. *Journal of Earthquake Engineering*, *27*(5), 1261–1280. https://doi.org/10.1080/13632469.2022.2074915

~~Hu, S., Hu, R., Yang, M., & Wang, T. (2023). Seismic behavior of the combined viscous-steel damping system for a long-span suspension bridge considering wave-passage effect. *Journal of Bridge Engineering*, *28*(7), 04023034. https://doi.org/10.1061/JBENF2.BEENG-5718~~

~~Hu, R., Hu, S., Yang, M., & Meng, D. (2023). Experimental study on the coordinated behavior of the Combined Viscous-Steel Damping System (CVSDS) for multi-level seismic mitigation. *Structures*, *57*, 105344. https://doi.org/10.1016/j.istruc.2023.105344~~

Hu, S., Yang, M., Zhang, H., Meng, D., & Li, X. (2024). Numerical and experimental study of a suspension bridge with combined viscous-steel damping system under train and seismic loads. *Structure and Infrastructure Engineering*, 1–14. https://doi.org/10.1080/15732479.2024.2335621 **AQ4**

Reply to AQ4：authors confirmed the citation is right. there is no information for the volume of this journal.
Hu, S., Yang, M., Zhang, H., Meng, D., & Li, X. (2024). Numerical and experimental study of a suspension bridge with combined viscous-steel damping system under train and seismic loads. Structure and Infrastructure Engineering, 1–14. https://doi.org/10.1080/15732479.2024.2335621

Zhou, L., Wang, X., & Ye, A. (2019). Shake table test on transverse steel damper seismic system for long span cable-stayed bridges. *Engineering Structures*, *179*, 106–119. https://doi.org/10.1016/j.engstruct.2018.10.073

Chen, L., Su, R., Hu, K., Ma, Z., Zhong, J., & Xiang, N. (2023). Probabilistic seismic evaluation and experimental tests of multi-direction damping system on a super-long column-pylon cable-stayed bridge. *Journal of Earthquake Engineering*, *27*(13), 3904–3927. https://doi.org/10.1080/13632469.2022.2153947

Hu, S., Yang, M., Meng, D., & Hu, R. (2023). Damping performance of the degraded fluid viscous damper due to oil leakage. *Structures*, *48*, 1609–1619. https://doi.org/10.1016/j.istruc.2023.01.070

Hu, S., Hu, R., Yang, M., & Wang, T. (2023). Seismic performance of the combined viscous-steel damping system suffering from oil leakage. *Journal of Vibration and Control*, *29*(21-22), 4885–4895. https://doi.org/10.1177/10775463221126028

Hu, S., Hao, H., Meng, D., & Yang, M. (2025). Theoretical and numerical study of the thermo-mechanical coupling effect on the fluid viscous damper. *Journal of Sound and Vibration*, *597*, 118846. https://doi.org/10.1016/j.jsv.2024.118846

Yang, M., Hu, R., Meng, D., & Zhang, H. (2024). A novel Horizontal Bidirectional Hybrid Damping System (HBHDS) for multi-level vibration control of long-span bridges: A theoretical study. *Engineering Structures*, *305*, 117693. https://doi.org/10.1016/j.engstruct.2024.117693

Hu, R., Yang, M., Meng, D., Cucuzza, R., & Domaneschi, M. (2024). Robustness investigation of Horizontal Bidirectional Hybrid Damping System applied to long-span bridges under near-fault pulse-like earthquakes. *Soil Dynamics and Earthquake Engineering*, *184*, 108803. https://doi.org/10.1016/j.soildyn.2024.108803

Suzuki, A., & Iervolino, I. (2020). Intensity measure conversion of fragility curves. *Earthquake Engineering & Structural Dynamics*, *49*(6), 607–629. https://doi.org/10.1002/eqe.3256

Meng, D., Liu, Q., Yang, M., & Yang, Z. (2023). Seismic vulnerability of simply-supported bridges considering link-slabs in the continuous deck and pounding. *Structure and Infrastructure Engineering*, *19*(10), 1459–1477. https://doi.org/10.1080/15732479.2022.2033279

Hu, Z., Wei, B., He, X., Jiang, L., & Li, S. (2022). Effects of spatial variation of ground motion (SVGM) on seismic vulnerability of ultra-high tower and multi-tower cable-stayed bridges. *Journal of Earthquake Engineering*, *26*(16), 8495–8524. https://doi.org/10.1080/13632469.2021.1991517

Wei, B., Zheng, X., Jiang, L., Lai, Z., Zhang, R., Chen, J., & Yang, Z. (2024). Seismic response prediction and fragility assessment of high-speed railway bridges using machine learning technology. *Structures*, *66*, 106845. https://doi.org/10.1016/j.istruc.2024.106845

Xiang, N., & Alam, M. (2019). Comparative seismic fragility assessment of an existing isolated continuous bridge retrofitted with different energy dissipation devices. *Journal of Bridge Engineering*, *24*(8), 04019070. https://doi.org/10.1061/(ASCE)BE.1943-5592.0001425

Casciati, F., Cimellaro, G., & Domaneschi, M. (2008). Seismic reliability of a cable-stayed bridge retrofitted with hysteretic devices. *Computers & Structures*, *86*(17-18), 1769–1781. https://doi.org/10.1016/j.compstruc.2008.01.012

Guo, J., Gao, K., Dang, X., Zheng, Y., & Liang, H. (2023). Seismic fragility assessment for highway bridges incorporating multi-level shape memory alloy cable dampers. *Engineering Structures*, *287*, 116172. https://doi.org/10.1016/j.engstruct.2023.116172

Zhang, H., Chen, Z., Hua, X., Huang, Z., & Niu, H. (2020). Design and dynamic characterization of a large-scale eddy current damper with enhanced performance for vibration control. *Mechanical Systems and Signal Processing*, *145*, 106879. https://doi.org/10.1016/j.ymssp.2020.106879

Ismail, M., Casas, J., & Rodellar, J. (2013). Near-fault isolation of cable-stayed bridges using RNC isolator. *Engineering Structures*, *56*, 327–342. https://doi.org/10.1016/j.engstruct.2013.04.007

Ernst, H. (1965). Der E-modul von seilen unter bercksichtigung des durchhanges. *Der Bauing*, *40*(2), 52–55.

Chadwell, C., & Imbsen, R. (2004). *XTRACT: A tool for axial force-ultimate curvature interactions*

[Paper presentation]. Structural ASCE Library. https://doi.org/10.1061/40700(2004)178

Guo, J., Gu, Y., Wu, W., Chu, S., & Dang, X. (2022). Seismic fragility assessment of cable-stayed bridges crossing fault rupture zones. *Buildings*, *12*(7), 1045. https://doi.org/10.3390/buildings12071045

Wang, H., Hu, R., Xie, J., Tong, T., & Li, A. (2013). Comparative study on buffeting performance of Sutong Bridge based on design and measured spectrum. *Journal of Bridge Engineering*, *18*(7), 587–600. https://doi.org/10.1061/(ASCE)BE.1943-5592.0000394

Park, J., & Otsuka, H. (1999). Optimal yield level of bilinear seismic isolation devices. *Earthquake Engineering & Structural Dynamics*, *28*(9), 941–955. https://doi.org/10.1002/(SICI)1096-9845(199909)28:9%3C941::AID-EQE848%3E3.0.CO;2-5

Wouterse, J. (1991). Critical torque and speed of eddy current brake with widely separated soft iron poles. *IEE Proceedings B Electric Power Applications*, *138*(4), 153–158. https://doi.org/10.1049/ip-b.1991.0019

Guo, T., Liu, J., Zhang, Y., & Pan, S. (2015). Displacement monitoring and analysis of expansion joints of long-span steel bridges with viscous dampers. *Journal of Bridge Engineering*, *20*(9), 04014099. https://doi.org/10.1061/(ASCE)BE.1943-5592.0000701

Zentner, I., Gündel, M., & Bonfils, N. (2017). Fragility analysis methods: Review of existing approaches and application. *Nuclear Engineering and Design*, *323*, 245–258. https://doi.org/10.1016/j.nucengdes.2016.12.021

Li, S., Wang, J., & Alam, M. (2021). Seismic performance assessment of a multispan continuous isolated highway bridge with superelastic shape memory alloy reinforced piers and restraining devices. *Earthquake Engineering & Structural Dynamics*, *50*(2), 673–691. https://doi.org/10.1002/eqe.3353

Jalayer, F., Ebrahimian, H., Miano, A., Manfredi, G., & Sezen, H. (2017). Analytical fragility assessment using unscaled ground motion records. *Earthquake Engineering & Structural*

Dynamics, *46*(15), 2639–2663. https://doi.org/10.1002/eqe.2922

Shafieezadeh, A., Ramanathan, K., Padgett, J., & DesRoches, R. (2012). Fractional order intensity measures for probabilistic seismic demand modeling applied to highway bridges. *Earthquake Engineering & Structural Dynamics*, *41*(3), 391–409. https://doi.org/10.1002/eqe.1135

Feng, R., Wang, X., Yuan, W., & Yu, J. (2018). Impact of seismic excitation direction on the fragility analysis of horizontally curved concrete bridges. *Bulletin of Earthquake Engineering*, *16*(10), 4705–4733. https://doi.org/10.1007/s10518-018-0400-2

Ma, K., Zhong, J., Feng, R., & Yuan, W. (2019). Investigation of ground-motion spatial variability effects on component and system vulnerability of a floating cable-stayed bridge. *Advances in Structural Engineering*, *22*(8), 1923–1937. https://doi.org/10.1177/1369433219827238

Wu, W., Li, L., & Shao, X. (2016). Seismic assessment of medium-span concrete cable-stayed bridges using the component and system fragility functions. *Journal of Bridge Engineering*, *21*(6), 04016027. https://doi.org/10.1061/(ASCE)BE.1943-5592.0000888

Wei, B., Hu, Z., He, X., & Jiang, L. (2020). Evaluation of optimal ground motion intensity measures and seismic fragility analysis of a multi-pylon cable-stayed bridge with super-high piers in mountainous areas. *Soil Dynamics and Earthquake Engineering*, *129*, 105945. https://doi.org/10.1016/j.soildyn.2019.105945

Zhong, J., Jeon, J., Shao, Y., & Chen, L. (2019). Optimal intensity measures in probabilistic seismic demand models of cable-stayed bridges subjected to pulse-like ground motions. *Journal of Bridge Engineering*, *24*(2), 04018118. http

Reply to AQ5：Theer is no information about volume number and page range because it is not a paper published in journal.

Hazus, M. H. (2011). Multi-hazard loss estimation methodology: Earthquake model hazus-MH MR5 technical manual. Federal Emergency Management Agency, Washington, DC, USA. AQ5

~~Wei, B., Wang, W. H., Wang, P., Yang, T., Jiang, L., & Wang, T. (2022). Seismic responses of a high-speed railway (HSR) bridge and track simulation under longitudinal earthquakes. *Journal of Earthquake Engineering*, 26(9), 4449–4470. https://doi.org/10.1080/13632469.2020.1832937~~

Zhong, J., Xu, W., & Wei, K. (2023). Quantifying site-response effect of spatial variability earthquake on seismic failure mode of long-span sea-crossing cable-stayed bridges. *Ocean Engineering*, *281*, 114839. https://doi.org/10.1016/j.oceaneng.2023.114839

Li, C., Li, H., Hao, H., Bi, K., & Chen, B. (2018). Seismic fragility analyses of sea-crossing cable-stayed bridges subjected to multi-support ground motions on offshore sites. *Engineering Structures*, *165*, 441–456. https://doi.org/10.1016/j.engstruct.2018.03.066

Choi, E., DesRoches, R., & Nielson, B. (2004). Seismic fragility of typical bridges in moderate seismic zones. *Engineering Structures*, *26*(2), 187–199. https://doi.org/10.1016/j.engstruct.2003.09.006

Author Query

1. **Query** [AQ0] : Please review the table of contributors below and confirm that the first and last names are structured correctly and that the authors are listed in the correct order of contribution. This check is to ensure that your names will appear correctly online and when the article is indexed.

Sequence	Prefix	Given name(s)	Surname	Suffix
1		Renkang	Hu	
2		Menggang	Yang	
3		Dongliang	Meng	
4		Shangtao	Hu	
5		Raffaele	Cucuzza	
6		Wenxi	Wang	
7		Marco	Domaneschi	

Response by Author: "Accepted"

2. **Query** [AQ1] : The disclosure statement has been inserted. Please correct if this is inaccurate.

Response by Author: "Accepted"

3. **Query** [AQ2] : Please provide full reference details for (Hu, Meng, Hu, & Yang, 2023a, 2023b, Hu, Yang, & Meng, 2023a, Meng, Liu, & Yang, 2023, and Bando Prin 2022) following journal style or delete the citations from the text.

Response by Author: "Answered within text"

4. **Query** [AQ3] : There is no mention of Reference (Hu et al. 2024, Hu et al. 2025 and Wei et al. 2022) in the text. Please cite the reference in the text or delete the references from the list.

Response by Author: "Answered within text"

5. **Query** [AQ4] : Please provide missing volume number for Hu et al., 2024 in the reference list.

   Response by Author: "Answered within text"

6. **Query** [AQ5] : Please provide missing volume number and page range for Hazus, 2011 in the reference list.

   Response by Author: "Answered within text"

7. **Query** [AQ6] : Please note that the ORCID section has been created from information supplied with your manuscript submission/CATS. Please correct if this is inaccurate.

   Response by Author: "Answered within text"

8. **Query** [AQ7] : The funding information provided has been checked against the Open Funder Registry and we failed to find a match. Please check and resupply the funding details if necessary.

   Response by Author: "Answered within text"

Author Approve Comments

1. **Author** [7/26/2025 4:32:25 AM] : The corresponding Author sent a note with a new Figure 5 in attachment. It does have a better resolution. Please replace Figure 5 with the new one.